

# Implementing the sine transform of fermionic modes as a tensor network

Hannes Epple,\* Pascal Fries, and Haye Hinrichsen

*Fakultät für Physik und Astronomie,  
Julius-Maximilians Universität Würzburg,  
Am Hubland, 97074 Würzburg, Germany*

(Dated: March 24, 2022)

Based on the algebraic theory of signal processing, we recursively decompose the discrete sine transform of first kind (DST-I) into small orthogonal block operations. Using a diagrammatic language, we then second-quantize this decomposition to construct a tensor network implementing the DST-I for fermionic modes on a lattice. The complexity of the resulting network is shown to scale as  $\frac{5}{4}n \log n$  (not considering swap gates), where  $n$  is the number of lattice sites. Our method provides a systematic approach of generalizing Ferris' spectral tensor network for non-trivial boundary conditions.

## I. INTRODUCTION

The study of tensor networks is currently a topic of growing interest both in condensed matter physics and quantum computation. In condensed matter physics, tensor networks can be used to model the entanglement structure of quantum states and are therefore well suited for the study of ground states of strongly correlated systems [1–3]. Specifically, the formulation of the *multiscale entanglement renormalization ansatz* (MERA) in this framework has shown to be very fruitful [3–6] and can be understood as a lattice realization of the *holographic principle* [7, 8], contributing to a better understanding of gauge-gravity type dualities [9]. In quantum computation, on the other hand, tensor networks are known as *quantum circuits* [10] and provide a natural framework for the decomposition of a large, complicated unitary operation into a sequence of small local building blocks – a simple example being the factorization of the *quantum Fourier transform* [10] into a sequence of Hadamard and phase gates, which causes the efficiency of Shor's algorithm [11].

A unification of both subjects—namely, the simulation of strongly correlated quantum systems by a quantum circuit—was already proposed by Feynman in 1982 [12] and has recently been realized by a circuit [13] for implementing the *exact* dynamics of free fermions on a circle. More recently, Ferris refined this idea [14], giving it the interpretation of a *spectral tensor network*, which implements the Fourier transform of *fermionic modes*, hence diagonalizes the Hamiltonian of free fermions [15]. Additionally, the geometry of this network generalizes to higher dimensions, while always staying easily contractible, such that it can be used for the *classical simulation* of phase transitions in more than one dimension – a feature that is absent in the MERA [16, 17].

The starting point for the construction of Ferris' spectral tensor network is a recursive algorithm for the discrete Fourier transformation (DFT), widely known as

Fast Fourier transform (FFT) [18]. The network is then chosen such that it implements the FFT in the one-particle sector of the theory [14]. This means that *every particle* is transformed separately, subject to the constraint of their respective indistinguishability. Note that this is entirely different from the quantum Fourier transform, which calculates a single DFT on the space spanned by all particles.

A closely related transformation, on which we will focus in the present work, is the discrete sine transformation of first kind (DST-I). This is a variant of the DFT for vanishing Dirichlet boundary conditions and thus indispensable for diagonalization procedures of systems on an open chain [15]. However, the boundary conditions break the convenient cyclic translational symmetry vital to the decomposition of the DFT, meaning that the original FFT algorithm can no longer be used.

The *algebraic theory of signal processing* [19, 20] tackles this problem by constructing an algebraic framework for spectral transformations. Based on these notions, decompositions of whole classes of transformations were derived in [21, 22], including the DST-I as a special case. However, in contrast to the simple case of the standard FFT, the resulting decomposition almost entirely consists of non-unitary elementary transformations. While this is acceptable for numerical recipes restricted to a single particle, we run into problems when translating the decomposition into a quantum circuit, implementing the transformation for indistinguishable particles.

In this paper we unitarize a recursive algorithm for the DST-I, originally given in [22], and show how to second-quantize the resulting algorithm, obtaining a spectral tensor network for a fermionic chain with open ends. To this end we reorganize the network in a non-trivial way. To keep the formal ballast as small as possible, the present paper explains most of the steps in terms of diagrams, showing selected parts of the decomposition and an explicit example of a complete algorithm.

\* hannes.epple@stud-mail.uni-wuerzburg.de

## II. THE FAST FOURIER TRANSFORM AND DIAGRAM NOTATION

The conventional discrete Fourier transform (DFT) converts a sequence of  $n$  complex numbers  $x_0, x_1, \dots, x_{n-1}$  into another sequence of complex numbers  $\tilde{x}_0, \tilde{x}_1, \dots, \tilde{x}_{n-1}$  by means of the linear transformation

$$\tilde{x}_a := \sum_{b=0}^{n-1} e^{-2\pi i ab/n} x_b.$$

Defining the phase factor  $\omega_n := e^{-2\pi i/n}$ , this transformation can be written as

$$\tilde{x} = \text{DFT}_n x \quad \text{with} \quad \text{DFT}_n^{ab} = \omega_n^{a \cdot b}.$$

Here and in the following, we use the convention that the lower index  $n$  denotes the dimension of the respective vector space, while upper indices  $0 \leq a, b < n$  label components of the matrix.

For even  $n = 2m$ , the recursion formula

$$\begin{aligned} \text{DFT}_{2m} &= L_{2m}(\text{DFT}_m \oplus \text{DFT}_m) \\ &\times (\mathbb{I}_m \oplus \text{diag}(\omega_{2m}^0, \dots, \omega_{2m}^{m-1})) (\text{DFT}_2 \otimes \mathbb{I}_m) \quad (1a) \end{aligned}$$

with

$$\bar{L}_{2m-1}^{ab} := \begin{cases} 1 & \text{iff } b \equiv am \pmod{2m-1} \\ 0 & \text{otherwise} \end{cases}$$

is known as the radix 2 fast Fourier transform (FFT) [18]. It factorizes the  $\text{DFT}_{2m}$  into three pieces: The rightmost factor  $\text{DFT}_2 \otimes \mathbb{I}_m$  is a basis transformation, consisting of  $m$  copies of the matrix

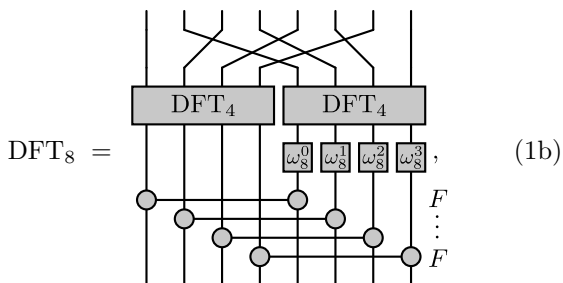
$$F := \text{DFT}_2 = \begin{pmatrix} 1 & 1 \\ 1 & -1 \end{pmatrix}$$

acting on the pairs of components  $(\ell, m + \ell)$ ,  $\ell = 0, \dots, m - 1$ . The next factor,

$$\text{DFT}_m \oplus \text{DFT}_m \text{ diag}(\omega_{2m}^0, \dots, \omega_{2m}^{m-1}),$$

is a direct sum of two  $DFT_m$ , one of which is modified by multiplication with a diagonal matrix of so called *twiddle factors*. The last factor  $L_{2m}$  just permutes the basis vectors, sorting them into odd and even portions.

Diagrammatically, the recursion relation (1a) for  $n = 8$  can be represented as



running from bottom to top. Here, blocks represent matrices, the ingoing lines are columns, while the outgoing lines are rows. The composition rules for such diagrams are

$$\begin{array}{c} \text{Box } B \\ \text{Box } A \end{array} = \text{Box } BA, \quad \begin{array}{c} \text{Box } C \\ \text{Box } D \end{array} = \text{Box } C \oplus D, \quad (2)$$

i.e., vertical composition couples rows of the lower block to columns of the upper block and therefore represents ordinary matrix multiplication, while horizontal composition gives rise to the direct sum of matrices [23]. Since the matrix  $F$  is applied to non-neighboring lines, we do not draw it as a box but rather use the shorthand notation

$$\begin{array}{c} \text{Diagram 1} \\ \text{Diagram 2} \end{array} = \begin{array}{c} \text{Diagram 3} \end{array} \quad (3)$$

with two bullets to indicate on which lines the matrix acts. Note that lines can be crossed arbitrarily, allowing us to move the remaining unaffected lines freely.

Now, if  $n$  is a power of 2, we can use eq. (1a), anchored at  $\text{DFT}_2 = F$ , to implement the  $\text{DFT}_n$  using only  $2 \times 2$ -matrices. In the above diagrammatic language, this amounts to having no blocks act on more than two lines. By construction, the number of blocks in such a diagram then scales as  $n \log_2 n$ , which therefore serves as an upper bound for the computational complexity of the DFT.

In order to interpret the DFT as a change of orthonormal bases in a single-particle Hilbert space, it needs to be unitary. This is achieved by the normalization

$$\widehat{\text{DFT}}_n := \frac{1}{\sqrt{n}} \text{DFT}_n$$

and, as can be easily checked, eqs. (1a) and (1b) remain valid under the replacement  $DFT \rightarrow \widehat{DFT}$ , provided we also normalize  $F$  by

$$F \rightarrow \hat{F} := \frac{1}{\sqrt{2}} F. \quad (4)$$

We thus obtain a decomposition of the large unitary  $\widehat{\text{DFT}}_n$  into small unitary building blocks, which again carry the interpretation of basis transformations in the single particle Hilbert space.

The process of second quantization [24] then maps the  $\widehat{\text{DFT}}_n$  to a basis change in the many-particle Hilbert space. Remarkably, the FFT scheme (1b) is still valid in the many-particle case, provided that we slightly change the composition rules (2) and replace the blocks by their respective second quantizations. We will discuss second quantization of Fourier transforms in more detail later in section V.

### III. DECOMPOSING THE DISCRETE SINE TRANSFORM

The discrete sine transform (DST) is a real linear transformation which captures essentially the imaginary part of the DFT. As it expands the data in sinusoids, this transformation is particularly useful for discrete systems with Dirichlet boundary conditions. However, depending on the implementation of the boundary conditions and the respective periodic continuation, one distinguishes various types of DSTs, which are usually labeled by Roman numbers from I to VIII [20].

We focus on the DST-I here, which corresponds to a periodic continuation that is odd around both  $x_{-1}$  and  $x_n$ . Thus, we have  $x_{-1} = x_n = 0$ , making the DST-I suitable for systems with open boundary conditions. As we will see below, for a suitable recursion scheme we also need the DST-III. The two DSTs are defined by the matrices

$$\text{DST-I}_n^{ab} = \sin \frac{(a+1)(b+1)\pi}{n+1} \quad \text{and} \quad (5)$$

$$\text{DST-III}_n^{ab} = \sin \frac{(a+\frac{1}{2})(b+1)\pi}{n}, \quad (6)$$

with  $0 \leq a, b < n$ , which are non-orthogonal. An advantage of considering the DST-I is that we only need the DST-III and the DST-I itself in the corresponding recursion. In principle, it is possible to consider other types of sine (or cosine) transforms and orthogonalize them in a similar way as described in the next section, though the corresponding recursions may be more complicated. Specifically, the DST-I of odd size  $n = 2m-1$  can be expressed recursively in terms of DST-I and DST-III as [22]

$$\begin{aligned} \text{DST-I}_{2m-1} = \\ \bar{L}_{2m-1} (\text{DST-III}_m \oplus \text{DST-I}_{m-1}) B_{2m-1}. \end{aligned} \quad (7a)$$

Here, the rightmost factor is a base change matrix

$$B_{2m-1} := \begin{pmatrix} \mathbb{I}_{m-1} & & \mathbb{J}_{m-1} \\ & 1 & \\ \mathbb{I}_{m-1} & & -\mathbb{J}_{m-1} \end{pmatrix}$$

with the  $(m-1) \times (m-1)$  identity matrix  $\mathbb{I}_{m-1}$  and

$$\mathbb{J}_{m-1} := \begin{pmatrix} & 1 \\ & \ddots \\ 1 & \end{pmatrix}.$$

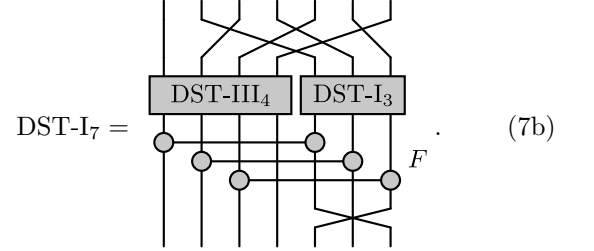
Note that  $B_{2m-1}$  can be split into an interaction part and a permutation,

$$B_{2m-1} = \begin{pmatrix} \mathbb{I}_{m-1} & & \mathbb{I}_{m-1} \\ & 1 & \\ \mathbb{I}_{m-1} & & -\mathbb{I}_{m-1} \end{pmatrix} \cdot \begin{pmatrix} \mathbb{I}_{m-1} & & \\ & 1 & \\ & & \mathbb{J}_{m-1} \end{pmatrix},$$

where the interaction part acts on pairs of components  $(\ell, m+\ell)$ ,  $\ell = 0, \dots, m-2$  via  $F$ . The middle factor is

just a direct sum of a DST-III and a DST-I of smaller sizes  $m$  and  $m-1$ , respectively, while the leftmost factor is a permutation defined in the previous section.

In the diagrammatic notation established before, the recursion relation (7a) for  $n = 7$  can be represented as



The DST-III appearing in this recursion can be further reduced by means of another recursion relation. For the DST-III of size  $n = 2m$  we use

$$\begin{aligned} \text{DST-III}_{2m} = & K_{2m} (\text{DST-III}_m \oplus \text{DST-III}_m) \\ & \times (X_m^- \oplus X_m^+) (\overline{\text{DST-III}}_2 \otimes \mathbb{I}_m) \bar{B}_{2m}, \end{aligned} \quad (8a)$$

which is a special case of a more general decomposition for  $n = qm$  [22]. Note that in contrast to the binary recursion (7a), the above formula recurs to two copies of DST-III itself. Again, the rightmost factor is a base change matrix

$$\bar{B}_{2m} := \begin{pmatrix} \mathbb{I}_{m-1} & \mathbb{J}_{m-1} \\ & 1 \\ & & \mathbb{I}_{m-1} \end{pmatrix} \oplus 1,$$

which leaves the components  $m-1$  and  $2m-1$  unaffected and applies the matrix

$$A := \begin{pmatrix} 1 & 1 \\ 0 & 1 \end{pmatrix}$$

to pairs of components  $(\ell, 2m-2-\ell)$ ,  $\ell = 0, \dots, m-2$ . Because of its tensor product structure, the next factor  $\overline{\text{DST-III}}_2 \otimes \mathbb{I}_m$  applies a scaled DST-III to pairs of components  $(\ell, m+\ell)$ ,  $\ell = 0, \dots, m-1$ , given by the matrix

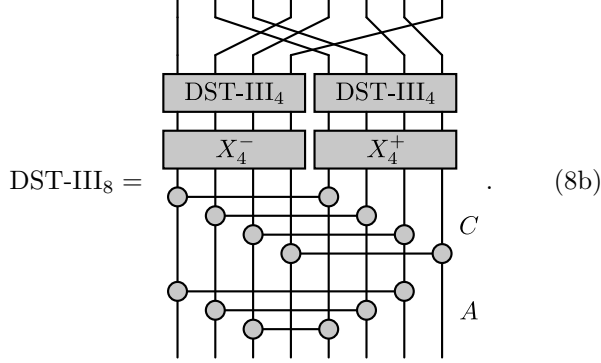
$$C := \overline{\text{DST-III}}_2 = F \text{diag}(1, \sqrt{2}).$$

The third factor in eq. (8a) is a direct sum of two matrices  $X_m^\pm$ , which will be discussed later on. The next factor consists of a direct sum of two smaller DST-IIIIs, while the leftmost factor is again a permutation, defined by

$$K_{2m} := (\mathbb{I}_2 \oplus \mathbb{J}_2 \oplus \mathbb{I}_2 \oplus \mathbb{J}_2 \oplus \dots) L_{2m}.$$

We can represent the recursion relation (8a) diagrammat-

ically as



The remaining parts to consider are the matrices  $X_m^\pm$ . For even size  $m$ , they are given by

$$X_m^\pm := \begin{pmatrix} c_m^1 & & s_m^{\pm(m-1)} & 0 \\ \ddots & & \ddots & \\ & c_m^{m/2} + s_m^{\pm m/2} & & \vdots \\ \ddots & & \ddots & \\ s_m^{\pm 1} & \dots & c_m^{m-1} & 0 \\ 0 & \dots & 0 & c_m^m \end{pmatrix} \quad (9)$$

with

$$c_m^\ell := \cos \frac{\ell\pi}{4m} \quad \text{and} \quad s_m^\ell := \sin \frac{\ell\pi}{4m}.$$

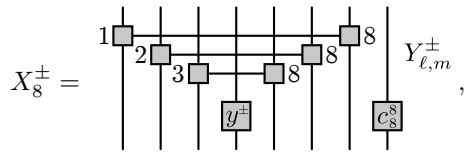
Clearly, these matrices can also be decomposed into blocks acting only on pairs of components  $(\ell-1, m-1-\ell)$ ,  $\ell = 1, \dots, m/2-1$  via

$$Y_{\ell,m}^\pm := \begin{pmatrix} c_m^\ell & s_m^{\pm(m-\ell)} \\ s_m^{\pm\ell} & c_m^{m-\ell} \end{pmatrix}. \quad (10)$$

Further, in the center and the right lower corner of the matrix (9), we have the factors

$$y^\pm := c_m^{m/2} + s_m^{\pm m/2} = \sqrt{1 \pm \frac{1}{\sqrt{2}}} \quad \text{and} \quad c_m^m = \frac{1}{\sqrt{2}},$$

acting on the components  $m/2-1$  and  $m-1$ . For example, the matrix  $X_m^\pm$  of size  $m=8$  can be drawn in our diagrammatic notation as



where the indices  $\ell$  and  $m$  of the  $2 \times 2$  matrices  $Y_{\ell,m}^\pm$  are given on the left and right of the corresponding symbol, respectively.

Putting all this together, the two mutually dependent recursions relations (7a) and (8a) together with the closing conditions

$$\text{DST-I}_1 = 1 \quad \text{and} \quad \text{DST-III}_2 = F \text{ diag} \left( \frac{1}{\sqrt{2}}, 1 \right)$$

allow us to calculate the DST-I of size  $n = 2^k - 1$  using only  $2 \times 2$  matrices. However, in the existing formulation, all the occurring matrices, except for permutations, are still non-orthogonal. This is a problem in the corresponding quantum version, since non-orthogonal building blocks cannot be interpreted as elementary changes of orthonormal bases. Fortunately, it is possible to reformulate the recursion relations in an orthogonal way, as will be shown in the next section.

#### IV. ORTHOGONALIZATION OF THE RECURSION RELATIONS

We now show step by step how to obtain an orthogonal version of the recursion relations (7a) and (8a) discussed in the previous section. For convenience, we label all orthogonal matrices by a hat symbol.

As stated before, the DSTs defined by eqs. (5) and (6) are non-orthogonal. However, all DSTs can be made orthogonal by a suitable scaling of rows and columns. Let us start with the DST-I. Multiplying the corresponding matrix (5) by its transpose, we find that the correct scaling is given by

$$\widehat{\text{DST-I}}_n := \text{DST-I}_n \sqrt{\frac{2}{n+1}}, \quad (11a)$$

meaning that all matrix entries are rescaled identically. Representing multiplication of a component by a small diamond this relation may be drawn as

$$\widehat{\text{DST-I}}_n = \begin{array}{c} \text{DST-I}_n \\ \diamond \quad \diamond \quad \diamond \end{array} \sqrt{\frac{2}{n+1}} \quad (11b)$$

in our graphical notation. Now we can try to recast the recursion (7a) in terms of orthogonal matrices. The procedure is shown in fig. 1 for a DST-I of size  $n = 2^{k+1} - 1$ .

The diagram on the left is just eq. (7b) with the proper scaling factors according to eq. (11) added at the bottom. In the first step, we split up the factors for each component and move factors of  $1/\sqrt{2^{k-1}}$  above the matrices  $F$ . This is possible since we have the same factor at every component. As no matrix  $F$  is acting on the component in the middle, we can also move the remaining factor of  $1/\sqrt{2}$  for this component further up, as indicated by the arrow. Now, all we have to do is to absorb all factors into the matrices directly above them. We obtain orthogonal matrices  $\hat{F}$  as defined in eq. (4). Further, the factors absorbed into the DST-I are just the ones from eq. (11), so

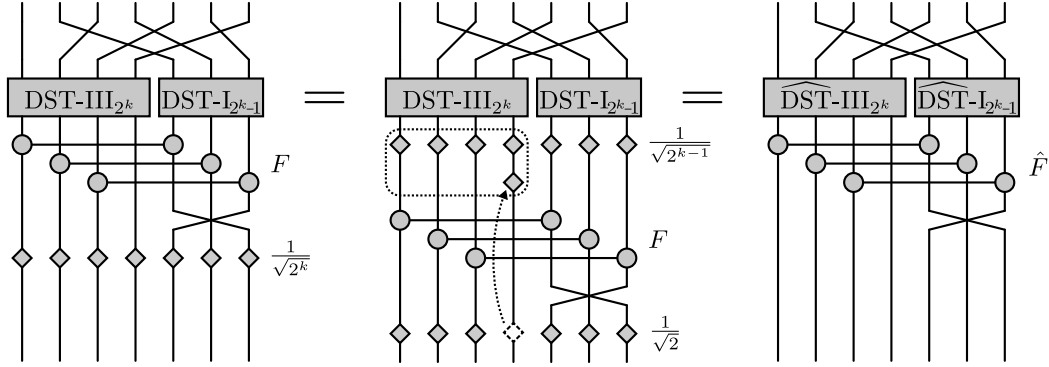


Figure 1. Orthogonalization of the recursion relation eq. (7a) for the DST-I of size  $n = 2^{k+1} - 1$ , shown here for  $k = 2$ .

we obtain an orthogonal version of this transform. Since we know that the whole transform in fig. 1 is orthogonal and all other building blocks are orthogonal, too, we can conclude that the DST-III together with the factors in the dotted box must also be orthogonal. Defining the orthogonalized DST-III as

$$\widehat{\text{DST-III}}_n := \text{DST-III}_n \sqrt{\frac{2}{n}} \text{ diag} \left( 1, \dots, 1, \frac{1}{\sqrt{2}} \right) \quad (12a)$$

or diagrammatically as

$$\widehat{\text{DST-III}}_n = \text{DST-III}_n \sqrt{\frac{2}{n}} \quad (12b)$$

we obtain the right diagram of fig. 1, where all occurring matrices are orthogonal.

Knowing the orthogonal version of the DST-III, we now turn to the corresponding recursion relation (8a). In a first step, we replace the DST-III by its orthogonal version, as it is shown in fig. 2 for a DST-III of size  $n = 2^{k+1}$ . We start with the recursion relation from eq. (7b) with scaling factors according to eq. (12) added at the bottom of the diagram. In the first step, we use eq. (12) to replace the two smaller DSTs by their orthogonal versions and the corresponding inverse scaling factors. Further, we express  $C = F \text{ diag}(1, \sqrt{2})$  in terms of  $\hat{F}$  using eq. (4). All factors except the ones in the dotted boxes cancel out. In the second step, we absorb those into the matrices below, obtaining the matrices

$$X'_m^\pm := \text{diag}(1, \dots, 1, \sqrt{2}) X_m^\pm \quad (13)$$

and  $A' := \text{diag}(1, \sqrt{2}) A$ ,

which unfortunately are still non-orthogonal. The part of the recursion relation that remains to be orthogonalized is indicated by a dashed box in the right diagram of fig. 2.

Let us have a look at  $X'_m^\pm$  first. The diagonal matrix in eq. (13) just cancels the factor  $c_m^m = 1/\sqrt{2}$  in the lower

right corner of  $X_m^\pm$ . Further, the occurring matrices  $Y_{\ell,m}^\pm$ , defined in eq. (10), can be decomposed as

$$Y_{\ell,m}^\pm = \hat{R}_{\pm\ell,m} Z^\pm,$$

with the rotation matrix

$$\hat{R}_{\ell,m} := \begin{pmatrix} \cos \frac{\ell\pi}{4m} & -\sin \frac{\ell\pi}{4m} \\ \sin \frac{\ell\pi}{4m} & \cos \frac{\ell\pi}{4m} \end{pmatrix}$$

and the non-orthogonal matrix

$$Z^\pm := \begin{pmatrix} 1 & \pm 1/\sqrt{2} \\ 0 & 1/\sqrt{2} \end{pmatrix}.$$

Thus, the diagrammatic representation of  $X'_m^\pm$ , drawn below for  $m = 8$ , is

$$X'_8^\pm = \begin{array}{c} \text{Diagram showing a 3x8 grid of boxes labeled 1, 2, 3, 8, 8, 8, 8, 8. A dashed box highlights a 2x2 block in the bottom-right corner. A dotted box highlights a 2x2 block in the middle-right column. Labels } \hat{R}_{\ell,m} \text{ and } Z^\pm \text{ are to the right.} \end{array}$$

Using this representation, the operations in the dashed box in the right diagram of fig. 2 can be redrawn as shown in the left diagram of fig. 3. We have doubled the number of components in this diagram to show all relevant structures and used the abbreviation  $m = 2^k$ . Again, the non-orthogonal part is highlighted by a dotted box.

In order to obtain the expression made up from orthogonal matrices given by the right diagram in fig. 3, we observe that the part in the dotted box can be decomposed into three sorts of blocks for any size  $n = 2^{k+1}$ . On the pair of components  $(2^k - 1, 2^{k+1} - 1)$ , we have a trivial block

$$\text{Diagram showing a simple connection between two components, labeled } \hat{F}.$$

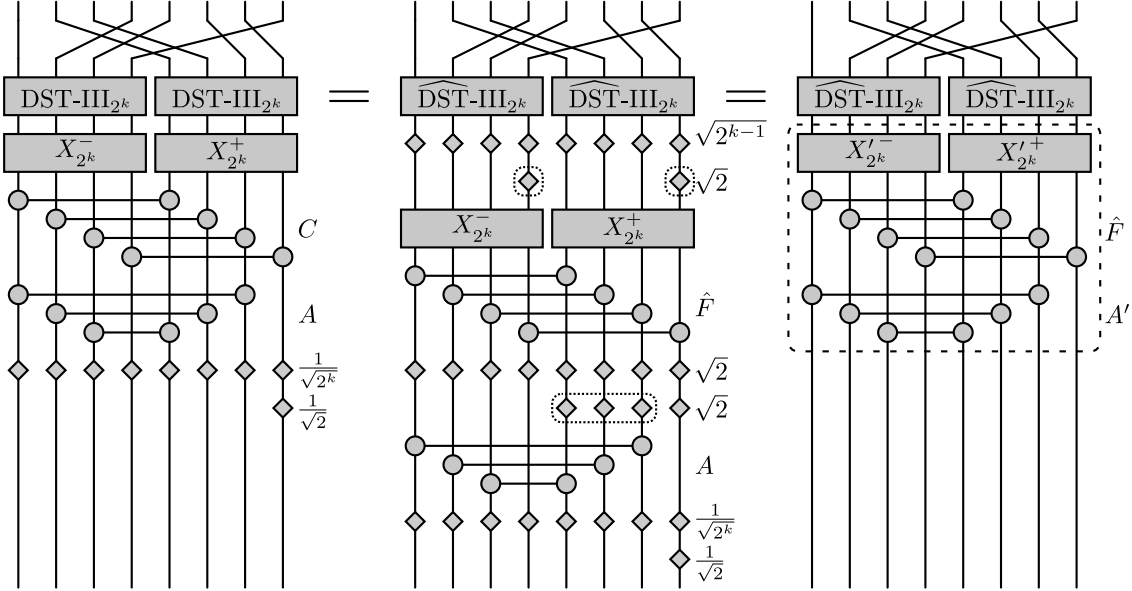


Figure 2. Orthogonalization of the recursion relation (8a) for the DST-III of size  $n = 2^{k+1}$ . Again, we have  $k = 2$ . The part in the dashed box in the right diagram is considered in fig. 3.

which is already orthogonal. Further, the pair of components  $(2^{k-1} - 1, 2^k + 2^{k-1} - 1)$  is coupled by

$$\begin{array}{c} y \\ \square \\ \square \\ \square \end{array} \otimes \begin{array}{c} y^* \\ \square \\ \square \\ \square \end{array} = -\frac{n}{2} \begin{array}{c} \square \\ \square \end{array} \otimes \begin{array}{c} \square \\ \square \end{array} \hat{R}_{\ell,m},$$

where the reformulation on the right hand side only contains matrices which are orthogonal. All other operations decompose into blocks acting on four components

$$(\ell, 2^k - 2 - \ell, 2^k + \ell, 2^{k+1} - 2 - \ell)$$

with  $\ell = 0, \dots, 2^{k-1} - 2$ . These blocks may be orthogonalized by the relation

$$\begin{array}{c} Z^- \\ \square \\ \square \\ \square \end{array} \otimes \begin{array}{c} Z^+ \\ \square \\ \square \\ \square \end{array} = \begin{array}{c} \square \\ \square \\ \square \\ \square \end{array} \otimes \begin{array}{c} \square \\ \square \\ \square \\ \square \end{array} \hat{F},$$

where we introduced the matrix

$$\hat{G} := \hat{F} \mathbb{J}_2 = \frac{1}{\sqrt{2}} \begin{pmatrix} 1 & 1 \\ -1 & 1 \end{pmatrix}.$$

Replacing the operations in the dashed box in the right diagram of fig. 2 by the right hand side of fig. 3 (in the appropriate size), we obtain a recursion relation for the DST-III that only contains orthogonal operations.

This completes all steps that are required to obtain a completely orthogonal recursion relation for the DST-I of size  $n = 2m - 1 = 2^{k+1} - 1$ . Let us summarize our final results: For the DST-I<sub>n</sub>, we arrive at a binary recursion, which can be represented diagrammatically, e.g. for  $n = 7$ , as

$$\widehat{\text{DST-I}}_7 = \begin{array}{c} \text{DST-III}_4 \quad \text{DST-III}_3 \\ \square \quad \square \\ \square \quad \square \\ \square \quad \square \\ \square \quad \square \end{array} \otimes \begin{array}{c} \square \\ \square \\ \square \\ \square \end{array} \hat{F}. \quad (14a)$$

For arbitrary odd size  $n = 2m - 1$ , this can also be expressed as

$$\widehat{\text{DST-I}}_{2m-1} = \bar{L}_{2m-1} (\widehat{\text{DST-III}}_m \oplus \widehat{\text{DST-I}}_{m-1}) \hat{M}_{2m-1}. \quad (14b)$$

Here, we defined the matrix

$$\hat{M}_{2m-1} = \frac{1}{\sqrt{2}} \begin{pmatrix} \mathbb{I}_{m-1} & \mathbb{J}_{m-1} \\ \mathbb{J}_{m-1} & -\mathbb{J}_{m-1} \end{pmatrix},$$

which is just the orthogonalized version of the matrix  $B_{2m-1}$  from the non-orthogonal relation (7a).

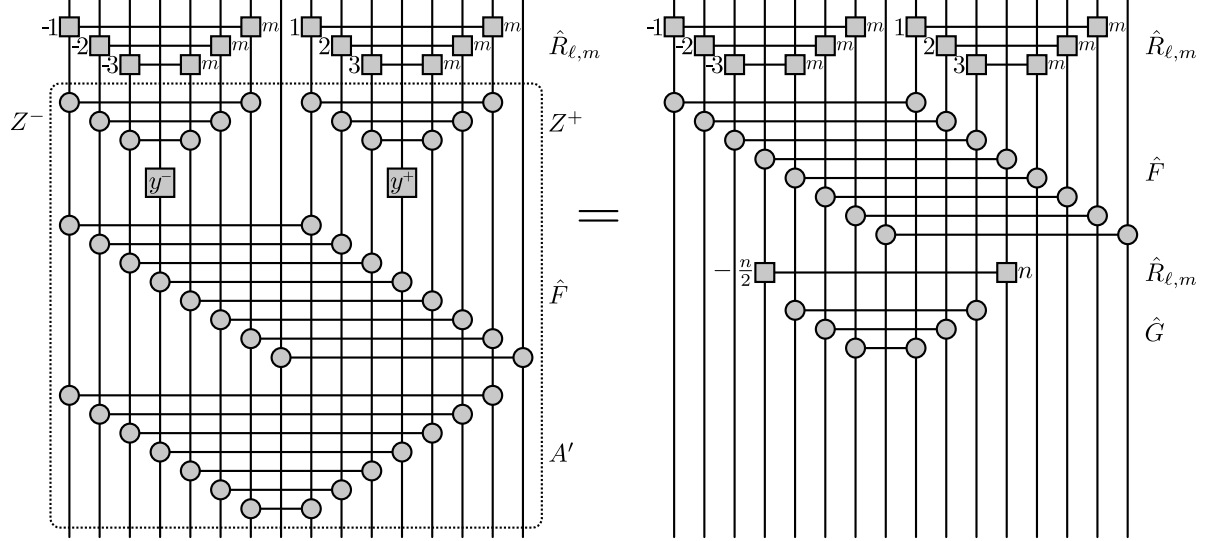
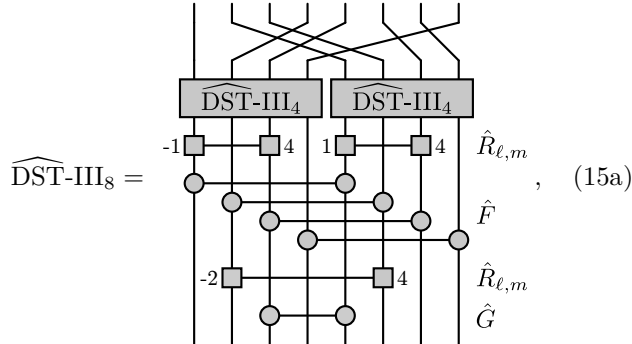


Figure 3. Detail for the orthogonalization of the recursion relation (8a) for the DST-III of size  $n = 2^{k+1}$ , shown here for  $k = 3$ , in order to resolve all relevant details. This figure corresponds to the part in the dashed box in the right diagram of fig. 2 with  $m = 2^k$ . The dotted box in the diagram on the left hand side of this figure indicates the part that remains to be reformulated in terms of orthogonal operations, as shown on the right hand side.

For the DST-III<sub>n</sub>, we found the diagram



which is given here as an example for  $n = 8$ . Again this has a general expression for  $n = 2m$ , given by

$$\widehat{\text{DST-III}}_{2m} = K_{2m} (\widehat{\text{DST-III}}_m \oplus \widehat{\text{DST-III}}_m) \times (\hat{Q}_m^- \oplus \hat{Q}_m^+) (\widehat{\text{DST-III}}_2 \otimes \mathbb{I}_m) \hat{N}_{2m}. \quad (15b)$$

The newly introduced matrix  $\hat{Q}_m^\pm$  is acting on pairs of components  $(\ell-1, m-1-\ell)$ ,  $\ell = 1, \dots, m/2-1$  via  $\hat{R}_{\pm\ell,m}$  and therefore has a similar structure as  $X_m^\pm$  defined in eq. (9). The other new matrix  $\hat{N}_{2m}$  couples the pair of components  $(m/2-1, 3m/2-1)$  by  $\hat{R}_{-m,2m}$  and the pairs of components  $(m/2-1+\ell, 3m/2-1-\ell)$ ,  $\ell = 1, \dots, m/2-1$  via  $\hat{G}$ .

The corresponding closing conditions for eqs. (14) and (15) are

$$\text{DST-I}_1 = 1 \quad \text{and} \quad \widehat{\text{DST-III}}_2 = \hat{F}, \quad (16)$$

such that the complete recursion leads to a well-defined network of operations. As an example, we drew the complete network for the  $\widehat{\text{DST-III}}_{31}$  in fig. 4.

To calculate the computational complexity of the derived algorithm, denote by  $\mathcal{C}_n^I$  and  $\mathcal{C}_n^{III}$  the number of elementary operations in the  $\widehat{\text{DST-III}}_n$  and  $\widehat{\text{DST-III}}_n$ , respectively, neglecting permutations. From eq. (14), we find

$$\mathcal{C}_{2^{k+1}-1}^I = \mathcal{C}_{2^k-1}^I + \mathcal{C}_{2^k}^{III} + (2^k - 1),$$

where the last summand is the number of  $\hat{F}$  matrices in each recursion step. On the other hand, eq. (15) implies

$$\mathcal{C}_{2^{k+1}}^{III} = 2\mathcal{C}_{2^k}^{III} + (2^k - 1) + 2^k + (2^k - 1),$$

the additional summands being the number of  $\hat{R}_{\ell,m}$ ,  $\hat{F}$ , and  $\hat{G}$  matrices per recursion step, in that order. Evaluating these formulae, anchored at  $\mathcal{C}_1^I = 0$  and  $\mathcal{C}_2^{III} = 1$ , we obtain

$$\mathcal{C}_n^I = \frac{5}{4}n \log_2(n+1) - \frac{13}{4}n + \frac{9}{4} \log_2(n+1) - \frac{1}{4} \quad (17a)$$

$$\text{and} \quad \mathcal{C}_n^{III} = \frac{5}{4}n \log_2 n - \frac{7}{4}n + 2. \quad (17b)$$

## V. SECOND QUANTIZATION OF DIAGRAMS

We will now outline a general method for performing second quantization of diagrammatic algorithms. We shall discuss fermions only – all results, however, extend naturally to the bosonic case [14, 25].

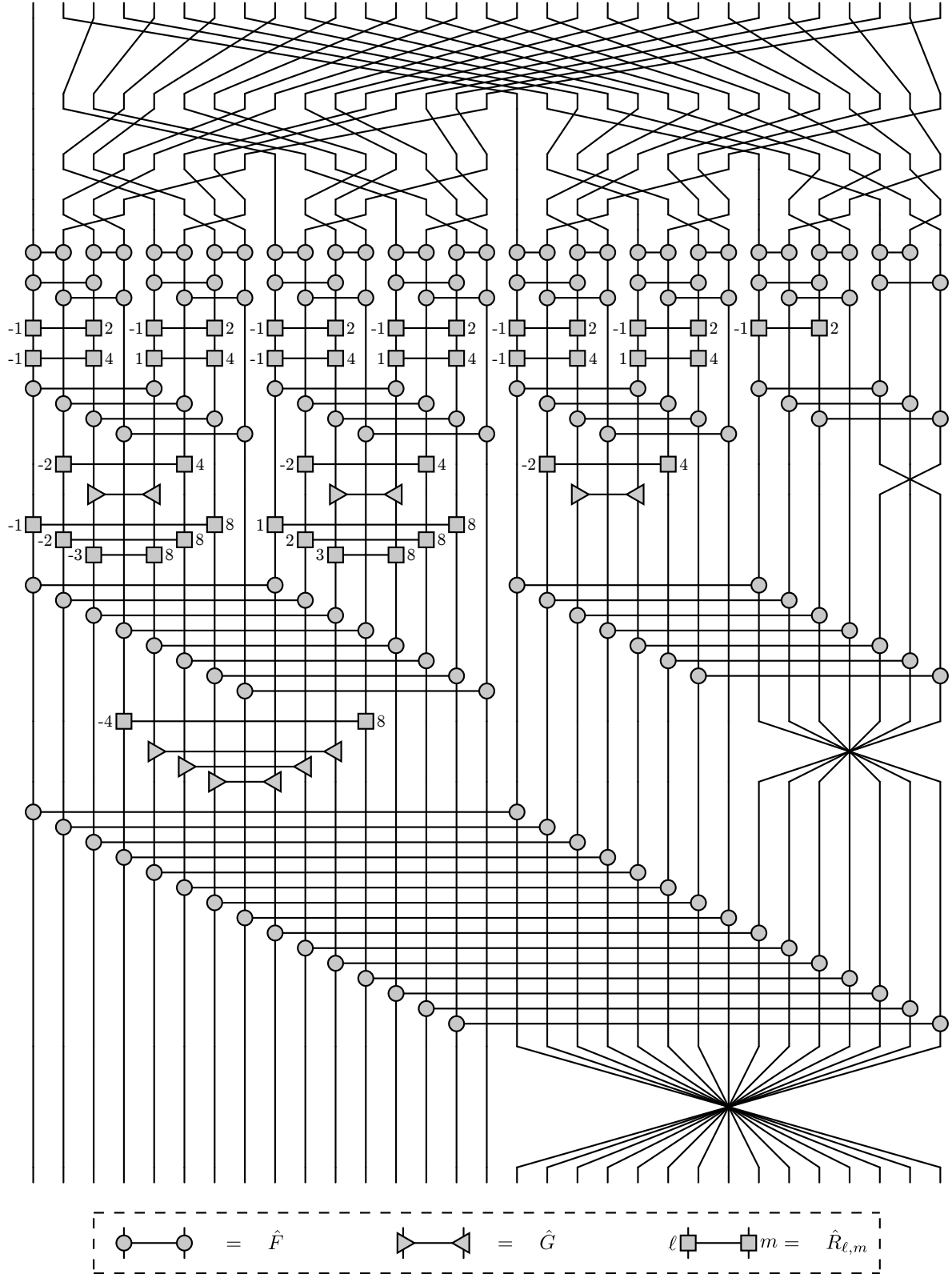


Figure 4. Diagrammatic representation of the  $\widehat{\text{DST}}\text{-I}_{31}$  made up entirely from orthogonal operations acting on only two components. The diagram is obtained from the recursion relations (14) and (15), together with the corresponding closing conditions (16).

Let us start with a basis transformation  $U$  on the single-particle Hilbert space. Its matrix representation is given by

$$U|a\rangle = \sum_b |b\rangle \langle b|U|a\rangle =: \sum_b U^{ba} |b\rangle. \quad (18)$$

We can extend  $U$  to a basis transformation  $\Gamma_U$  of the multi-particle Hilbert space, by having it leave the vacuum  $|\Omega\rangle$  invariant and act linearly on creation operators  $c^\dagger$  [25, 26]. This means that in the occupation number basis

$$|k\rangle = (c_0^\dagger)^{k_0} \cdots (c_{n-1}^\dagger)^{k_{n-1}} |\Omega\rangle, \quad k_a \in \{0, 1\},$$

we define the *second quantization*  $\Gamma_U$  of  $U$  by

$$\Gamma_U |k\rangle := (c_{U|0\rangle}^\dagger)^{k_0} \cdots (c_{U|n-1\rangle}^\dagger)^{k_{n-1}} |\Omega\rangle, \quad (19)$$

where the transformed mode

$$c_{U|a\rangle}^\dagger := \sum_b U^{ba} c_b^\dagger \quad (20)$$

creates a fermion in the state  $U|a\rangle$ .

Similarly to eq. (18), we then have

$$\Gamma_U |k\rangle = \sum_l \Gamma_U^{lk} |l\rangle,$$

where eqs. (19) and (20) can be used to obtain

$$\begin{aligned} \Gamma_U^{lk} &= \left\langle \Omega \left| c_{n-1}^{l_{n-1}} \cdots c_0^{l_0} \left( \sum_{b_0} U^{b_0 0} c_{b_0}^\dagger \right)^{k_0} \cdots \right. \right. \\ &\quad \times \left. \left. \left( \sum_{b_{n-1}} U^{b_{n-1} n-1} c_{b_{n-1}}^\dagger \right)^{k_{n-1}} \right| \Omega \right\rangle. \end{aligned} \quad (21)$$

Denote now by

$$\begin{aligned} L &= (L_0, \dots, L_{p_l-1}) := \{a | l_a = 1\} \quad \text{and} \\ K &= (K_0, \dots, K_{p_k-1}) := \{a | k_a = 1\} \end{aligned}$$

the (ordered) lists of occupied modes in  $|l\rangle$  and  $|k\rangle$ , respectively, where  $p_l$  and  $p_k$  are their total numbers. Obviously, we have  $\Gamma_U^{lk} = 0$  for  $p_l \neq p_k$ , since then the modes in eq. (21) do not match up in pairs. Let us thus consider the case where  $p_k = p_l =: p$ . Here, we have

$$\begin{aligned} \Gamma_U^{lk} &= \sum_{b_0, \dots, b_{p-1}} U^{b_0 K_0} \cdots U^{b_{p-1} K_{p-1}} \\ &\quad \times \left\langle \Omega \left| c_{L_{p-1}} \cdots c_{L_0} c_{b_0}^\dagger \cdots c_{b_{p-1}} \right| \Omega \right\rangle, \end{aligned}$$

where the expectation value on the right hand side again vanishes if  $(b_0, \dots, b_{p-1}) \neq L$  as sets. Since the summand also changes sign under odd permutations of  $(b_0, \dots, b_{p-1})$ , we obtain

$$\begin{aligned} \Gamma_U^{lk} &= \sum_{\pi \in S_p} \text{sgn}(\pi) U^{L_{\pi(0)} K_0} \cdots U^{L_{\pi(p-1)} K_{p-1}} \\ &= \det((U^{L_b K_a})_{0 \leq a, b < p}), \end{aligned} \quad (22)$$

which shall serve as a recipe for the calculation of  $\Gamma_U$ .

The Slater determinant expression (22) enables us to check the functorial relations [25]

$$\Gamma_{UU'} = \Gamma_U \Gamma_{U'} \quad \text{and} \quad \Gamma_{U \oplus U'} = \Gamma_U \otimes \Gamma_{U'}. \quad (23)$$

Also, we see that second quantization preserves unitarity and orthogonality, since

$$\Gamma_{U^\dagger} = \Gamma_U^\dagger, \quad \Gamma_{U^\text{T}} = \Gamma_U^\text{T}, \quad \text{and} \quad \Gamma_{\mathbb{I}_n} = \mathbb{I}_{2^n}.$$

We can now use eq. (23) to second-quantize the diagrams from the preceding sections. This amounts to replacing all single particle matrices  $U$  by their respective second quantizations  $\Gamma_U$ . Each vertical line then represents an occupation number, hence the vertical composition of blocks as on the left hand side of eq. (2) turns into a tensor contraction

$$\sum_{k_3, k_4} \Gamma_B^{k_1 k_2, k_3 k_4} \Gamma_A^{k_3 k_4, k_5 k_6} = (\Gamma_B \Gamma_A)^{k_1 k_2, k_5 k_6},$$

while the right hand side turns into the tensor product

$$\Gamma_C^{k_1 k_2, k_3 k_4} \Gamma_D^{k_5 k_6, k_7 k_8} = (\Gamma_C \otimes \Gamma_D)^{k_1 k_2 k_5 k_6, k_3 k_4 k_7 k_8}.$$

Note that this does not affect the *structure* of the diagrams at all, but just amounts to a reinterpretation of what they are supposed to mean.

Since only scalars  $\alpha$  and  $2 \times 2$ -matrices  $U$  appear in the diagrams we use, we can explicitly evaluate eq. (22) to obtain

$$\Gamma_\alpha = \begin{pmatrix} 1 & 0 \\ 0 & \alpha \end{pmatrix} \quad \text{and} \quad (24)$$

$$\Gamma_U = \begin{pmatrix} 1 & & & \\ & U^{11} & U^{10} & \\ & U^{01} & U^{00} & \\ & & & \det U \end{pmatrix}. \quad (25)$$

in the Kronecker basis  $\{|00\rangle, |01\rangle, |10\rangle, |11\rangle\}$ .

Finally, we have to give a meaning to the crossings of vertical lines, as in eq. (3). For a single particle, these are represented by the swap matrix

$$S := \begin{pmatrix} 0 & 1 \\ 1 & 0 \end{pmatrix},$$

hence in the multi-particle case, we can apply eq. (25) to find

$$\Gamma_S = \begin{pmatrix} 1 & & & \\ & 0 & 1 & \\ & 1 & 0 & \\ & & & -1 \end{pmatrix}, \quad (26)$$

which correctly picks up a negative sign if two fermions switch places.

As an example, consider the normalized version of the FFT diagram in eq. (1b). We can recursively break it

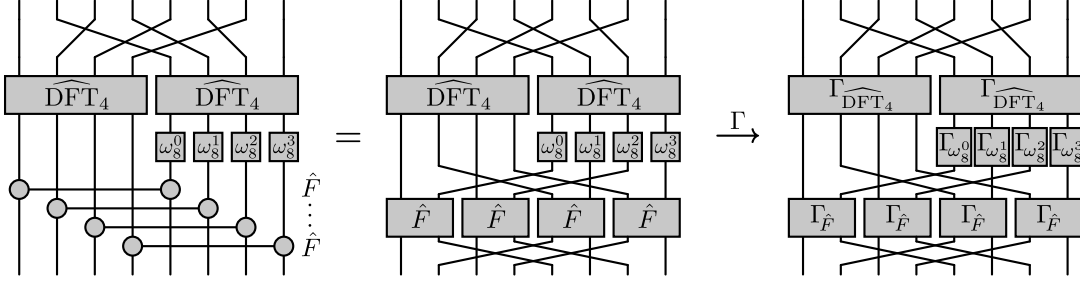


Figure 5. Second quantization of the FFT diagram from eq. (1b). First, we unravel the shorthand notation (3). Then each block is replaced by its second quantization via eqs. (24) and (25). The overall structure of the diagrams is unchanged because of the functorial relations eq. (23), however, whenever two lines cross, we have to insert the fermion swap gate  $\Gamma_S$ , obtained in eq. (26).

down, so that we only need the second quantization of  $\hat{F}$  from eq. (4), given by the matrix

$$\Gamma_{\hat{F}} = \begin{pmatrix} 1 & & & \\ -1/\sqrt{2} & 1/\sqrt{2} & & \\ 1/\sqrt{2} & 1/\sqrt{2} & & \\ & & & -1 \end{pmatrix}$$

and local terms as in eq. (24). The entire process can be found in fig. 5, resulting in a diagram that exactly reproduces the *spectral tensor network* by [13, 14]. Correspondingly, we can use the same rules on the unitary decompositions (14) and (15) derived in the preceding section, to obtain a quantum circuit implementing the DST-I for fermions and thus generalizing the spectral tensor network for open boundary conditions. Therefore, eq. (17) gives an upper bound for the *quantum computational complexity* [10] of the DST-I and DST-III of fermionic modes. Note, however, that we omitted any permutations in the calculation leading to eq. (17). While this is fine if we deal with just a single particle, exchange statistics need to be incorporated for multiple fermions, hence permutations need to be decomposed into gates of type (26). This leads to additional  $\sim \frac{7}{6}n^2$  gates, where the coefficient arises from the most naive decomposition and can likely be dropped to a smaller value.

## VI. DISCUSSION

The present work is based on previous work by Püschel and Moura, who gave a purely algebraic framework for the study of spectral transformations for various types of boundary conditions [19, 20] and their recursive decomposition into sparse matrices [21, 22]. Although this work is remarkable and very general, its practical use for quantum mechanics is limited in so far as the building blocks of the resulting decomposition are not unitary – a crucial property of any transformation which is to be interpreted as a change of orthonormal bases in a Hilbert space. Since unitary variants of these Fourier transforms exist, it is of course near at hand to expect that also the

corresponding recursion relations can be reformulated in terms of unitary building blocks, but carrying out such a unitarization could be quite cumbersome.

In this paper, we have used a diagrammatic language to explicitly demonstrate said unitarization at the example of a discrete sine transformation. This led to a decomposition where the sparse matrices are direct sums of unitary elementary operations, hence well suited for parallelization. We expect that other generalized Fourier transformations can be made unitary in a similar way, although then the technicalities are probably even more involved.

The fact that the resulting recursion relations consist of block-diagonal unitaries is particularly important when turning to many particles in the context of second quantization. We have shown that such a second-quantized version of a sine transformation for fermions can be obtained by replacing the unitary building blocks of the diagram by appropriate second-quantized counterparts and suitable modifications for line crossings, to implement the particle statistics [3]. Doing so, we arrive at a tensor network, whose structure is essentially the same as that of the original diagram, a circumstance that has already been noted in the context of the ordinary DFT on a circle by Ferris [14].

Another great advantage of unitary building blocks becomes apparent when calculating local expectation values with the resulting tensor network: as in the case of the MERA, a causal structure emerges [4] and parts of the network that are not causally connected to the considered region can be contracted to trivial operations. Therefore, the effective complexity of the computation of one- and two-point functions drops even further, scaling just linearly with the system size.

The network thus makes it possible to numerically study boundary effects in one dimensional free fermion models, which are exactly solvable by means of a spectral transformation. The Jordan-Wigner transformation extends the applicability to spin- $\frac{1}{2}$  models, such as the XY model [15]. Imposing the variational method on the tensor coefficients, while fixing the overall topology, the proposed network could also provide a starting point for

the simulation of a wider class of models with non-cyclic boundary conditions. Furthermore, since Ferris' similar construction for the DFT naturally generalizes to higher dimensions, we expect that this also holds for the DST-I.

Finally, the observation that second quantization pre-

serves the structure of diagrams, which can be seen as some kind of *Bohr correspondence principle* on a higher level, seems to be very fundamental and is linked to the underlying category theory, as we shall discuss in a forthcoming paper.

---

[1] J. Eisert, in *Emergent Phenomena in Correlated Matter, Modeling and Simulation*, Vol. 3, edited by E. Pavarini, E. Koch, and U. Schollwöck (Forschungszentrum Jülich, Jülich, 2013) p. 520.

[2] R. Orús, *Ann. Phys.* **349**, 117 (2014), arXiv:1306.2164 [cond-mat.str-el].

[3] R. Orús, *The European Physical Journal B* **87**, 280 (2014), arXiv:1407.6552 [cond-mat.str-el].

[4] G. Vidal, *Phys. Rev. Lett.* **101**, 110501 (2008), arXiv:quant-ph/0610099.

[5] G. Evenbly and G. Vidal, *Phys. Rev. B* **79**, 144108 (2009), arXiv:0707.1454 [cond-mat.str-el].

[6] P. Corboz and G. Vidal, *Phys. Rev. B* **80**, 165129 (2009), arXiv:0907.3184 [cond-mat.str-el].

[7] L. Susskind, *J. Math. Phys.* **36**, 6377 (1995), arXiv:hep-th/9409089.

[8] B. Swingle, *Phys. Rev. D* **86**, 065007 (2012), arXiv:0905.1317 [cond-mat.str-el].

[9] J. Maldacena, *Adv. Theor. Math. Phys.* **2**, 231 (1998), arXiv:hep-th/9711200.

[10] M. A. Nielsen and I. L. Chuang, *Quantum Computation and Quantum Information* (Cambridge University Press, 2000).

[11] P. W. Shor, *SIAM J. Comp.* **26**, 1484 (1997), arXiv:quant-ph/9508027.

[12] R. P. Feynman, *International Journal of Theoretical Physics* **21**, 467 (1982).

[13] F. Verstraete, J. I. Cirac, and J. I. Latorre, *Phys. Rev. A* **79**, 032316 (2009), arXiv:0804.1888 [quant-ph].

[14] A. J. Ferris, *Phys. Rev. Lett.* **113**, 010401 (2014), arXiv:1310.7605 [quant-ph].

[15] E. Lieb, T. Schultz, and D. Mattis, *Ann. Phys.* **16**, 407 (1961).

[16] G. Evenbly and G. Vidal, *Phys. Rev. Lett.* **112**, 220502 (2014), arXiv:1205.0639 [quant-ph].

[17] G. Evenbly and G. Vidal, *Phys. Rev. Lett.* **112**, 240502 (2014), arXiv:1210.1895 [quant-ph].

[18] J. W. Cooley and J. W. Tukey, *Mathematics of Computation* **19**, 297 (1965).

[19] M. Püschel and J. Moura, *IEEE Trans. Sig. Proc.* **56**, 3572 (2008), arXiv:cs.IT/0612077.

[20] M. Püschel and J. Moura, *IEEE Trans. Sig. Proc.* **56**, 3586 (2008), arXiv:cs.IT/0612077.

[21] M. Püschel and J. Moura, *SIAM J. Comp.* **32**, 1280 (2003).

[22] M. Püschel and J. Moura, *IEEE Trans. Sig. Proc.* **56**, 1502 (2008), arXiv:cs.IT/0702025.

[23] Note that this is in strict contrast to the usual diagrammatics of tensor networks and stems from the fact that we are not considering multiple particles yet. This will change in section V, where horizontal composition will give rise to the tensor product. We thank the referee for suggesting to emphasize this point.

[24] F. A. Berezin, *The Method of Second Quantization* (Academic Press Inc, 1966).

[25] J. Dereziński and C. Gérard, *Mathematics of Quantization and Quantum Fields* (Cambridge University Press, 2013).

[26] N. N. Bogolyubov, *Nuovo Cimento* **7**, 794 (1958).